JOURNAL OF SOLID STATE CHEMISTRY **121,** 457–466 (1996)
ARTICLE NO. 0063

Optical and Crystallographic Study of Eu^{3+} and Tb^{3+} Doped $LiYO_2$: Phase Transition, Luminescence Efficiency and Crystal Field Calculation

M. D. Faucher,* O. K. Moune,* M-G Alves,* B. Piriou,* Ph. Sciau,† and M. Pham-Thi‡

*Laboratoire de Chimie et Physico-Chimie Moléculaire et Minérale, URA 1907 du CNRS, Ecole Centrale Paris, 92295 Châtenay-Malabry Cedex, France; †Laboratoire de Chimie Physique du Solide, URA 453 du CNRS, Ecole Centrale de Paris, 92295 Châtenay-Malabry Cedex, France; and ‡Thomson-CSF, LCR, Domaine de Corbeville, 91404 Orsay Cedex, France

Received May 23, 1995; in revised form October 3, 1995; accepted October 5, 1995

Crystallographic and optical studies were undertaken on powder samples of $LiYO_2$ doped with Eu^{3+} and Tb^{3+}. At room temperature, the compounds are monoclinic. A slight rise of the temperature or small quantities of a smaller cation (Tb^{4+}) induces a phase transition to a tetragonal form. The radiant efficiencies are 0.33 and 0.47 those of the commercial red and green TV standards $Y_2O_2S:Eu^{3+}$ and ZnS:Cu,Al, respectively. While stable at room temperature, the compounds do decompose into the oxides as the temperature is raised above 250°C. The ^7F multiplet and the lowest ^5D energy levels of the Eu^{3+} ($4f^6$) and the Tb^{3+} ($4f^8$) configurations are determined. Experimentally fitted crystal field parameters are compared to predicted parameters.

I. INTRODUCTION

The compounds Li*Ln*O2 exist in at least four structural forms depending on the lanthanide radius:

—α form: tetragonal, isotypic with $LiInO_2$ (distorted $LiFeO_2$) (space group: $I4_1/amd$), preferred by small lanthanides: *Ln* = Lu, Yb, Er. They were first studied by Hoppe *et al.* (1, 2), and Bertaut and Gondrand (3). A single-crystal structure refinement of $YbLiO_2$ was recently carried out by Glaum *et al.* [4].

—β form: monoclinic (space group: $P2_1/c$), exists for medium sized lanthanide ions: *Ln* = Y, Ho, Dy. These compounds were also reported in Ref. (3), and later examined in detail by Stewner and Hoppe (5).

—γ form: orthorhombic (space group: *Pbnm*), *Ln* = Tb, Gd, Eu, Sm. This form was also pointed out by Sevost'yanova *et al.* (6), Bärnighausen (7), and Gondrand (8, 9).

—δ form: monoclinic (space group: $P2_1/c$), *Ln* = Sm, Nd, Pr, La (10–12).

—A rhombic phase is pointed out in Ref. (6) but not confirmed by subsequent work.

The nomenclature of the different forms which was at first contradictory among the different authors has been clarified in Ref. (13). The effect of pressure was examined by Waintal and Gondrand (13). Preparation conditions of the rare earth doped lithium lanthanates were examined by Zaitsev *et al.* (Pr^{3+}, Tb^{3+}, Er^{3+}, Lu^{3+}) (14) and their hygroscopicity and some luminescent characteristics were reported by Rozdin *et al.* (Nd^{3+}, Eu^{3+}) (15). Lithium yttriate preferably adopts the α and β forms.

Europium doped into lithium yttriate with a distorted $LiFeO_2$ structure exhibits bright luminescence under 254 nm ultra-violet excitation. In the course of a search for efficient europium doped phosphors, Blasse *et al.* (16–18) investigated the alkaline rare earth hosts $LiGdO_2$, $NaGdO_2$, and $LiYO_2$. In these compounds, the activator excitation occurs by direct absorption of the radiation in a charge transfer process from the ligand to the rare earth ion. The quantum efficiency under 250–270 nm excitation was found equal to 50 and 80% for europium doped $LiYO_2$ and $NaGdO_2$, respectively, while the maximum quantum efficiency in the UV region was 65 and 80%, respectively (17). In Ref. (15), it is pointed out that in 93% moisture conditions, the weight increase of $LiYO_2$, $LiGdO_2$, $NaYO_2$, $NaGdO_2$, and KYO_2 is equal to 3, 45, 86, 84, and 180% respectively. Its good quantum yield designated $LiYO_2:Eu^{3+}$ as a promising new phosphor and prompted applied studies (19, 20) for the design of new cathode-ray tubes. It was found that 5% Eu^{3+} doped $LiYO_2$ is 1.5 times more efficient than a commercial batch of europium doped YVO_4 under cathode-ray excitation. The phosphor is stable under cathode-ray bombardment but decomposes into Y_2O_3 through heating with hydrocarbons.

Few spectroscopic studies can be found, such as for Eu^{3+} doped into Li*M*O_2 (with *M* = Sc, Lu, Y, and Gd) (Ref. 21, 22). The energy levels and a crystal field analysis of Nd^{3+} in $LiYO_2$ single crystals and some other spectroscopic properties are reported in Refs. (23, 24), while those of Dy^{3+} are investigated in Ref. (25) with some contradictions

0022-4596/96 $18.00

concerning the assignment of energy levels. In a preceding paper (26) we reported that the room-temperature monoclinic form of the 5% europium doped compound transforms to the tetragonal form at 350 ± 5 K.

Furthermore, the dielectric behavior of the $LiYO_2$ phases was examined and an antiferroelectric phase transition from the monoclinic (β form) to the tetragonal (α form) at 1170 K was reported some years ago (27, 28).

Reasons prompting a reexamination of the fluorescence properties of $LiYO_2$:Ln^{3+} compounds in relation to a precise determination of their crystal structure are:

—the significant efficiency of their luminescence as generally reported in earlier papers;

—the close-to-room-temperature phase transition and associated modifications of their physical properties.

—the search for the relations between the structural changes and the modifications of the optical spectra; and

—the possibility of a precise crystal field analysis in two different but closely related structural forms.

This paper is dedicated to the study of the luminescence and crystal structure of $LiYO_2$ doped with 5% Eu^{3+} and Tb^{3+}. For the europium doped compound, the properties are investigated below and above the phase transition.

Section II hereafter deals with the synthesis, the stability of the compounds, and the symmetry of their unit cells. Section III describes the structures and their relationships and gives the cell parameters and refined atomic positions. Section IV presents the experimental fluorescence data. Evaluated *ab initio* crystal field parameters based on structural data are compared to empirically fitted crystal field parameters in Section V.

II. SYNTHESIS, SYMMETRY, AND STABILITY OF THE DOPED COMPOUNDS

Starting materials were oxalic acid, lithium carbonate 99%, Y_2O_3, Eu_2O_3, and Tb_4O_7 99.9%, from Johnson Matthey. The $LiY_{0.95}(Eu, Tb)_{0.05}O_2$ powder samples were prepared by precipitating a mixed (Ln = Y + Eu or Ln = Y + Tb) rare earth chloride solution with oxalic acid according to the reaction

$$2LnCl_3 + 3(COOH)_2 + 10H_2O \rightarrow Ln_2(C_2O_4)_3 \cdot 10H_2O + 6HCl$$

(in an aqueous solution, the oxalate with $10H_2O$ is formed (29)). The precipitate was then washed, dried, and fired in an alumina crucible with an excess of lithium carbonate at 960°C for 2 h at the ordinary pressure and atmosphere. The compound was slowly cooled to room temperature. The compacted sample was scraped to eliminate the part of the powder which was in contact with the alumina crucible. The europium compound is white and the as-obtained terbium compound is light orange, due to the presence of Tb^{4+}. Heating for 30 h at 600°C in a reducing ($0.95Ar + 0.05H_2$) atmosphere converted it to Tb^{3+}. The resulting powder sample is white.

TABLE 1

Cell Symmetry of the $LiY_{1-x}Ln_xO_2$ Compounds at 300 K (Ln = rare earth) and Percent Decomposition after 2 h Heating at 260°C in Room Atmosphere

Ln	x	R_{Ln}(Å)	R_m(Å)	Symmetry	% Y_2O_3
Tb^{4+}	0.05	0.760	0.894	T	n
Pr^{4+}	0.05	0.850	0.898	T	10
Yb^{3+}	0.05	0.868	0.898	T //	9
Er^{3+}	0.05	0.890	0.899	M	80
Tb^{3+}	0.05	0.923	0.901	M	n
Y^{3+}	1	0.900	0.900	M	5
Eu^{3+}	0.05	0.947	0.902	M	14
Pr^{3+}	0.05	0.990	0.905	M	n

Note. Ln is the rare earth dopant, x its molar concentration, R its ionic radius in CN = 6 following Ref. (29), and R_m the mean heavy metal radius. M = monoclinic, $P2_1/c$: T = tetragonal, $I4_1/amd$. n denotes not investigated.

If we assume that in $LiYO_2$:Tb^{4+} all the oxygen and heavy metal sites are occupied, then some lithium sites have to be vacant and the compound formula is $Li^+_{0.95}[\ ]_{0.05}Y^{3+}_{0.95}Tb^{4+}_{0.05}O_2$. It belongs to the tetragonal α-form while the powder diffraction patterns of the Eu^{3+} and Tb^{3+} doped compound at room temperature show the lines of monoclinic β-$LiYO_2$ only. Table 1 gives the symmetry of the three compounds under study ($LiYO_2$:Eu^{3+}, $LiYO_2$:Tb^{3+}, $LiYO_2$:Tb^{4+}) of pure $LiYO_2$, and of some other doped compounds; the oxidation state and the concentration of the dopant; its effective ionic radius (30) for a coordination number CN = VI; the phase symmetry; and the mean heavy metal radius R_m which we assume is given by

$$R_m = ((1-x)\cdot R^3_{Y^{3+}} + x\cdot R^3_{Ln})^{1/3} \approx R_{Y^{3+}}\cdot\left(1+\frac{x}{3}\cdot\left(\left(\frac{R_{Ln}}{R_{Y^{3+}}}\right)^3-1\right)\right) \quad [1]$$

(for x small and $R_{Ln} \approx R_{Y^{3+}}$) as a function of Shannon's effective ionic radii and the molar dopant concentration x. Table 1 shows that the tetragonal phase occurs for a mean heavy metal ionic radius lower than 0.899 Å.

In the preparation of $LiYO_2$, an excess of lithium carbonate was introduced in order to obtain a compound free from the oxide Y_2O_3. However, after the synthesis, when the compound is heated again at 260°C, it decomposes slowly but steadily into Y_2O_3 and Li_2O. The approximate amount of Y_2O_3 after 2 h heating was estimated by scaling the ratio between the measured intensities of two diffrac-

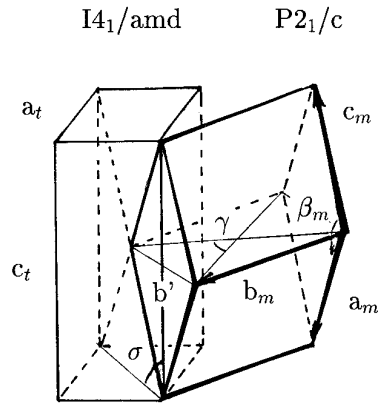

FIG. 1. Monoclinic and tetragonal forms of $LiYO_2$:*Ln*.

tion lines of $LiYO_2$ and Y_2O_3 respectively by the ratio of the theoretical intensities.

Table 1 lists the approximate amount of yttrium oxide present in three doped compounds after 2 h heating at 260°C. The maximum amount of decomposition occurs for the 5% erbium doped compound which is just about at the limit between the two crystalline forms. No systematic study of the decomposition on the whole set of compounds has been undertaken yet.

III. CRYSTALLOGRAPHIC INVESTIGATION

III.1. Cell Parameters of $LiYO_2:Eu^{3+}$ below and above the Phase Transition, $LiYO_2:Tb^{3+}$ and $LiYO_2:Tb^{4+}$ at Room Temperature

$LiYO_2:Eu^{3+}$ is monoclinic at temperatures below 350 K, and tetragonal above (25). The transition is reversible. With a 5% Tb content, $LiYO_2:Tb^{3+}$ is monoclinic and $LiYO_2:Tb^{4+}$ tetragonal. In both cases the differences between the two crystalline forms are minute. The mutual arrangement of the tetragonal and monoclinic cells is shown in Fig. 1. From geometrical considerations, it is easy to deduce the relations between the tetragonal and monoclinic parameters. a_{mt}^2 and c_{mt}^2 are the approximate a and c values deduced from the monoclinic parameters:

$$c_{mt}^2 = a_m^2 + c_m^2 - 2a_m c_m \cos\beta_m$$
$$a_{mt}^2 = (a_m^2 + b_m^2 + c_m^2 + 2a_m c_m \cos\beta_m)/4.$$

The square basal tetragonal plane is transformed into a parallelogram; b_m shortens and b' lengthens. b' (Fig. 1) is given by

$$b'^2 = a_m^2 + c_m^2 + 2a_m c_m \cos\beta_m.$$

The angle γ_{mt} is different from 90° and such as

TABLE 2

Cell Symmetry, Cell Parameters (Å), Approximate Tetragonal Parameters in the Monoclinic Phase, Volumes (Å^3), and Relative Variations between (1) the Low and High Temperature Forms of $LiY_{0.95}Eu_{0.05}O_2$ and (2) the $LiYO_2:Tb^{3+}$ and $LiYO_2:Tb^{4+}$ Structural Forms at Room Temperature

		1 $LiYO_2:Eu^{3+}$ (300 K)	2 $LiYO_2:Tb^{3+}$ [a] (300 K)
Monoclinic	a_m	6.1270(3)[b]	6.141(2)
	b_m	6.1924(3)	6.198(3)
	c_m	6.2133(2)	6.225(1)
	β_m	118.739(3)	118.79(1)
	a_{mt}	4.412	4.417
	c_{mt}	10.625	10.643
	Volume	206.75	207.65
		$LiYO_2:Eu^{3+}$ (370 K)	$LiYO_2:Tb^{4+}$ [a] (300 K)
Tetragonal	a_t	4.4478(2)	4.4116(6)
	c_t	10.3755(5)	10.400(1)
	Volume	205.29	202.44
	$100\ \Delta a_t/a_t$	0.8	−0.1
	$100\ \Delta c_t/c_t$	−2.4	−2.3
	$100\ \Delta V/V$	−0.8	−2.5

[a] Assumed compositions: $LiYO_2:Tb^{3+} = Li^+Y^{3+}_{0.95}Tb^{3+}_{0.05}O_2$ and $LiYO_2:Tb^{4+} = Li^+_{0.95}[\ ]_{0.05}\ Y^{3+}_{0.95}Tb^{4+}_{0.05}O_2$.

[b] The standard deviations between parentheses are obtained by the Rietveld (profile) refinement method and should be multiplied by 3.7 to obtain the probable errors.

$$\text{tg}\,\gamma_{mt}/2 = b'/b_m.$$

The c_{mt} axis bends down following a [110] direction so that angle σ (shown in Fig. 1) is equal to

$$\sigma = a\cos[(c_{mt}^2 - a_m^2)/(a_m^4 + c_m^4 - 2a_m^2 c_m^2 \cos 2\beta_m)^{1/2}] \neq 90°.$$

The correspondences between monoclinic and tetragonal plane indices are given by the following transformation matrix:

$$hkl_T = 1/2 \begin{vmatrix} 1 & 1 & 1 \\ 1 & -1 & 1 \\ -2 & 0 & 2 \end{vmatrix} hkl_M.$$

The cell parameters for $LiYO_2:Eu^{3+}$ below and above the phase transition were refined from the powder diffraction diagrams. They are reported in Table 2 column 1 with the approximate tetragonal cell parameters a_{mt} and c_{mt} derived from the monoclinic cell, the cell volumes, and the relative variations.

The same comparative analysis was done for $LiY_{0.95}Tb^{3+}_{0.05}$ (monoclinic phase) and $Li^{+}_{0.95}[\ ]_{0.05}Y^{3+}_{0.95}Tb^{4+}_{0.05}O_2$ (tetragonal phase). The cell parameters for the two crystallographic forms refined from the powder diffraction diagrams are given in Table 2, column 2. It can be stated, by comparing columns 1 and 2 in Table 2, that whether the phase transition occurs by varying the temperature or by modifying the mean heavy metal ionic radius, the variations of a_t are smaller than the relative change of c_t (about −2.3%). For the two terbium phases, the comparison is clear-cut, no thermal expansion can be invoked since the structural analyses are carried out at 300 K. a_t remains unchanged and only c_t is affected; it is shorter in the tetragonal phase, causing a 2.3% shrinking of the cell volume. At room temperature, the tetragonal phase occurs when the mean heavy metal radius falls below a critical value (about 0.899 Å). For a given composition, the phase transition occurs when the temperature rises, which means that the critical factor is not just the mean heavy metal radius but the ratio between the latter and the oxygen radius.

III.2. Crystal Structure Refinement of $LiYO_2:Eu^{3+}$ above the Phase Transition, and $LiYO_2:Tb^{4+}$ at Room Temperature

Since the crystal structure of the tetragonal form depends on one position parameter only (z_{oxygen}), it seems possible to determine it with a powder sample. The structure of the 5% europium doped compound at 110°C, above the phase transition, and that of the terbium doped compound (tetragonal form) at room temperature were investigated by means of a precise experimental design (5–2000 K) developed at Laboratoire de Chimie Physique du Solide (Ecole Centrale Paris). Preliminary measurements showed that the quality of the diagram of the europium compound was improved if the latter was annealed for 15 min at 500 K prior to the intensity measurements at 380 K. The intensity data of both phases were analyzed by the means of a profile fitting program XND developed by Bérar and Garnier (31). The background was defined by linear interpolation between 7 (2θ/intensity) points. Allowance was made for the correct intensity ratio between the Cu$K\alpha$1 and Cu$K\alpha$2 radiations utilized in all the experiments.

The space group proposed earlier ($I4_1/amd$) was confirmed and the refined atomic positions are listed in Table 3.

The purity of the phases was checked by X-ray diffraction only. A small percentage (6%) of cubic Y_2O_3 was detected in the europium compound, due to the short pre-

TABLE 3

Refined Atomic Positions and Isotropic Temperature Factors in (1) the High Temperature Form of $LiY_{0.95}Eu_{0.05}$ and (2) the $LiYO_2:Tb^{4+}$ Structural Form at Room Temperature

			1 $LiYO_2:Eu^{3+}$ (370 K)	2 $LiYO_2:Tb^{4+}$ [a] (300 K)
Tetragonal ($I4_1/amd$)	Yttrium (4*a*)	$x = y = z$	0.	0.
		B	0.73(4)	2.25[b](6)
	Lithium (4*b*)	$x = y$	0.	0.
		z	0.5	0.5
		B	3.4(6)	2.25[b](6)
	Oxygen (8*e*)	$x = y$	0.	0.
		z	0.2226(4)	0.2163(4)
		B	1.2(4)	2.25[b](6)
		R_{wp}	12.1	8.2
		R_B	6.5	4.4

[a] See footnote *a* in Table 2.
[b] Overall isotropic B factor.

TABLE 4

Trichromatic Coordinates and Luminous Conversion of $LiYO_2$ Doped with 5% Eu^{3+} and Tb^{3+} and of Television Standards $Y_2O_2S:Eu^{3+}$ and ZnS:Cu,Al under Cathodic Excitation (25 kV, 1 μW/Cm^2)

	/stand.	*x*	*y*
$Y_2O_2S:Eu^{3+}$	1.00	0.643	0.348
$LiYO_2:Eu^{3+}$ [a]	0.33	0.656	0.340
$LiYO_2:Eu^{3+}$ [b]	0.09	0.647	0.348
ZnS:Cu,Al	1.00	0.298	0.589
$Y_2O_2S:Tb^{3+}$	0.50	0.35	0.56
$LiYO_2:Tb^{3+}$ [a]	0.47	0.351	0.586
$LiYO_2:Tb^{3+}$ [b]	0.19	0.351	0.586
$Y_2O_3:Tb^{3+}$	0.11	0.330	0.574

[a] Screens obtained by sedimentation in alcohol.
[b] Screens prepared by sedimentation from an aqueous solution containing barium acetate and potassium silicate followed by a heat treatment in air at 400°C for 2 h.

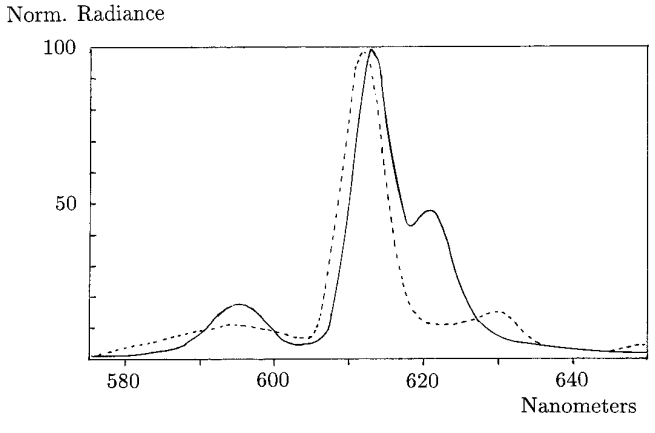

FIG. 2. Normalized radiance of $LiYO_2:Eu^{3+}$. Full lines, before heat treatment; dashed lines, after the screen forming process (decomposed into $Y_2O_3:Eu^{3+}$).

liminary annealing period. The corresponding intensities were substracted from the experimental data. No yttrium oxide nor any other extra phase was detected in the terbium data. If there were some lithium carbonate left in the samples, it was in too small quantities to be detected by X-ray diffraction.

IV. FLUORESCENCE—EXPERIMENTAL

$LiYO_2:Eu^{3+}$ illuminated with the 254 nm line of a mercury lamp emits a strong red luminescence originating from the $^5D_0 \rightarrow {}^7F_2$ transition. Under the same conditions $LiYO_2:Tb^{3+}$ emits a strong green luminescence due to the $^5D_4 \rightarrow {}^7F_5$ transition.

Table 4 reports the values of the luminescent conversion and the trichromatic coordinates of both materials under cathodic excitation (25 kV, 1 μW/cm^2) compared to television standards $Y_2O_2S:Eu^{3+}$ and ZnS:Cu,Al. The optimum luminescent conversion for $LiYO_2:Eu^{3+}$ and $LiYO_2:Tb^{3+}$ under cathodoluminescence was obtained with layers deposited from a suspension of the powder in ethylic alcohol dried at ordinary temperature. For the europium and terbium compound, the efficiency is 0.33 and 0.47 times that of the commercial standards, respectively. Regarding the trichromatic coordinates, red $LiYO_2:Eu^{3+}$ performs slightly better than $Y_2O_2S:Eu^{3+}$ (displaced toward the edge of the diagram) while green $LiYO_2:Tb^{3+}$ is worse (yellower) than ZnS:Cu,Al, therefore restricting the chromatic display area.

The efficiency of both phosphors drops significantly during the screen forming process in which the phosphor layers are deposited from an aqueous solution of barium acetate and potassium silicate and heated at 400°C for 2 h. Figure 2 shows the emission spectrum of $LiYO_2:Eu^{3+}$before and after the thermal treatment (spectral resolution = 2.5 nm). The emission spectrum has changed and obviously, the material has completely decomposed into $Y_2O_3:Eu^{3+}$ which is confirmed by X-ray diffraction. This fact was already pointed out by Jaffe and Konitzer for the europium doped compound (Ref. 20).

TABLE 5
Number of Allowed and Observed Transitions in a D_{2d} Site Symmetry

Initial level	Final level	Theoretical	Observed
$^5D_0 \rightarrow$	$^7F_0$	0	0
	$^7F_1$	2	2
	$^7F_2$	2	2
	$^7F_3$	3	3
	$^7F_4$	3	3
	$^7F_5$	4	3
	$^7F_6$	5	4
$^5D_1 \rightarrow$	$^7F_0$	2	2
	$^7F_1$	3	3
	$^7F_2$	6	6
	$^7F_3$	8	6
	$^7F_4$	10	5
$^5D_2 \rightarrow$	$^7F_0$	2	2

Similarly, Fig. 3 shows the emission spectrum of $LiYO_2:Tb^{3+}$ before and after the thermal treatment. This time, the emission lines between 480 and 630 nm do not shift at all which means that the material is not significantly decomposed but turns from white to orange indicating a partial oxidation of Tb^{3+} to Tb^{4+}. The luminous conversion also decreases drastically.

The degradation of the two phosphors during the screen forming process seems therefore to proceed differently: the europium doped compound dissociates into the oxides Y_2O_3 and Li_2O while some Tb^{3+} is oxidized into Tb^{4+}.

A detailed spectroscopic analysis was performed on both compounds.

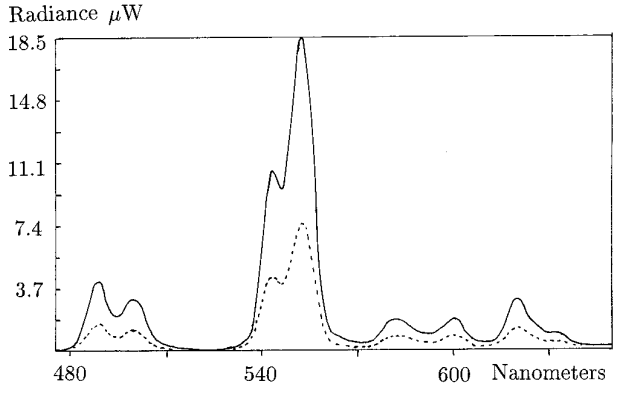

FIG. 3. Radiance of $LiYO_2:Tb^{3+}$. Full lines, before heat treatment; dashed lines, after the screen forming process.

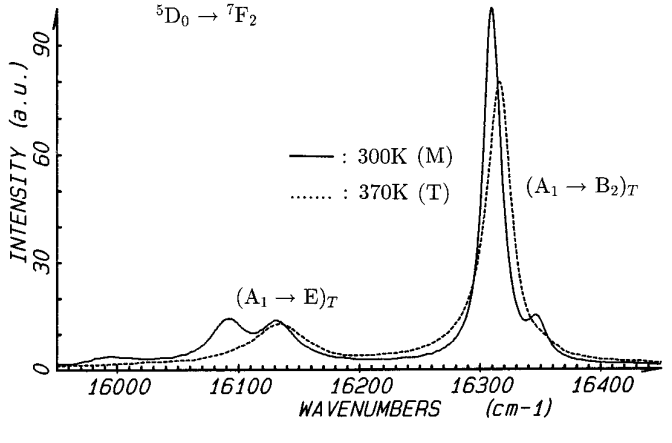

FIG. 4. Variation of the $^5D_0 \rightarrow {}^7F_2$ transition intensity of LiYO2:Eu^{3+} with temperature.

TABLE 6
Experimental and Calculated Energy Levels (in cm^{-1}) of $LiYO_2:Eu^{3+}$ at 77, 300, and 370 K

	77 K		300 K		370 K		
	Exp.	Cal.	Exp.	Cal.	Exp.	Cal.	Rep.
$^7F_0$	0	0	0	0	0	0	A_1
$^7F_1$	285	270	270	257	211	216	A_2
	349	351	381	382	438	434	E
	396	409	410	421			
$^7F_2$	821	816	838	826	847	843	A_1
	858	851	872	871	885	878	B_2
	1034	1036	1047	1054	1069	1069	E
	1091	1095	1089	1089			
	1154	1161	1186	1197	1281	1297	B_1
$^7F_3$	1807	1789	1827	1807	1807	1800	B_1
	1879	1892	1871	1879	1861	1844	B_2
	1934	1936	1953	1965	1973	1967	E
	1971	1972	1985	1986			
	1989	1990	2006	2007	/	2005	A_2
	2003	2001	2026	2030	2110	2125	E
	2018	2025	/	2048			
$^7F_4$	2637	2633	2664	2656	2712	2692	E
	2667	2657	2685	2672			
	2749	2747	2771	2764	/	2724	B_1
	2966	2974	2981	2993	/	3033	A_1
	3049	3051	3072	3076	/	3124	A_2
	3091	3079	3095	3095	3125	3127	B_2
	3104	3105	3127	3125	3191	3216	E
	3120	3128	3138	3139			
	3148	3154	3163	3172	3266	3255	A_1
$^7F_5$	3782	3791	3788	3780	3767	3774	E
	3808	3813	3788	3794			
	3841	3833	/	3842	/	3902	A_2
	3858	3861	3877	3864		3942	A_1
	3875	3881	3877	3881	3942	3943	E
	3896	3886	3877	3889			
	3921	3920	3907	3916	/	3951	B_2
	/	3927	/	3941	3951	3956	B_1
	4237	4235	4247	4240	4361	4352	E
	/	4252	4247	4252			
	4271	4269	4291	4279	/	4381	A_2
$^7F_6$	4812	4818	4811	4824	4779	4804	B_2
	4844	4847	/	4847	/	4838	B_1
	4890	4894	4952	4961	/	5020	A_1
	4916	4921	/	4986	5042	5043	E
	4949	4956	5013	5010			
	4992	4984	/	5042	/	5089	B_2
	/	5273	/	5315	5452	5461	E
	/	5282	/	5322			
	/	5338	5387	5379	/	5519	A_2
	5365	5362	/	5406	/	5543	B_1
	/	5388	/	5429	5578	5555	E
	5449	5451	/	5479			
	5471	5455	5499	5485	/	5569	A_1
$^5D_0$	17161		17177		17201		A_1
$^5D_1$	18897		18907		18918		A_2
	18908		18927		18952		E
	18916						
$^5D_2$	21287		21316		21331		E
	21298		/		/		
	21303		/		/		
	21452		21473		21503		B_2
$^5D_3$	24162						
	24184						
	24202						
	24218						
	24312						

IV.1. $LiYO_2:Eu^{3+}$

The compound contains an unique site available for the yttrium (europium) ions. Several techniques were utilized to measure the ^7F_J and ^5D_J ($J = 0, 1, 2, 3$) levels of Eu^{3+} ($4f^6$ configuration) up to 24300 cm^{-1}.

—Fluorescence under continuous ultraviolet (254 nm) excitation of a low pressure mercury lamp (Vilber Lourmat). All the $^5D_J \rightarrow {}^7F_J$ fluorescence lines are recorded in the same time.

—Fluorescence under pulsed selective excitation of one of the $^5D_2$ levels of Eu^{3+}. The tunable dye (coumarin) laser is pumped by the 355 nm radiation of a YAG laser associated with a KDP crystal. Nonradiative processes populate the lower ^5D_J ($J = 0, 1$) levels so that the light emitted by the sample contains the ^5D_J ($J = 0, 1, 2$) $\rightarrow$ $^7F_{J'}$ ($J' = 0, 1, 2, 3, 4, 5, 6$) lines. It is analyzed in a 0.8-m double grating spectrometer (Coderg company, model PHO) equipped with a R928 Hamamatsu photomultiplier followed by a digitalscope (Tektronix 2430). The corresponding pulsed signal is processed by a BFM 187 personal computer where it is stored. Its treatment (delay, gate, accumulation, amplification) permits one to select the lines originating from each ^5D_J level (32). Since the lifetimes of the ^5D_J levels of the Eu^{3+} ion are such as $\tau_0 \gg \tau_1 \gg \tau_2$, the condition is roughly $t_{\text{delay}}(J) = 2(\tau_{J+1})$; $t_{\text{gate}}(J) = 1.5(\tau_J)$. This multiple time selection requires only a single scan.

—An excitation spectrum is performed with the same setup. The spectrometer wavelength is adjusted on the strongest $^5D_0 \rightarrow {}^7F_2$ line while the energy of the exciting dye laser is tuned to sweep across the $^5D_2$ region. The resulting spectrum displays the $^7F_0 \rightarrow {}^5D_2$ lines.

The experiments were carried out at 77, 300, and 370 K. At 77 and 300 K, the site symmetry of europium is C_1

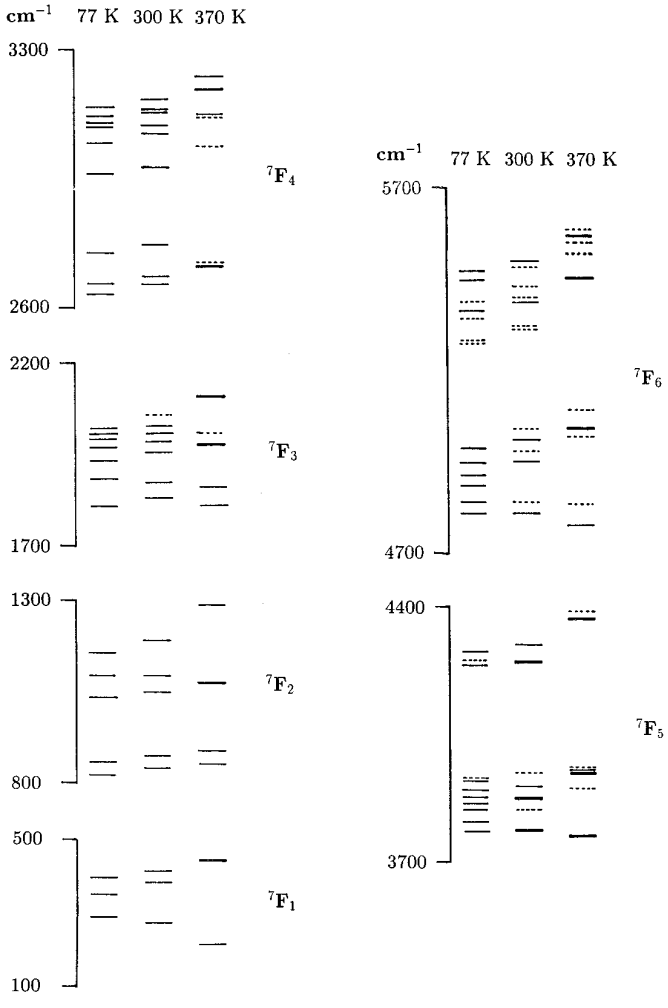

FIG. 5. Energy levels of $LiYO_2$:Eu^{3+} at 77, 300, and 370 K.

and the degeneracy of the ^7F_J sublevels is completely lifted. All the energy levels have the same symmetry label A_1. At 77 K, 43 out of the 49 ^7F_J levels are detected. The spectral lines shift continuously between 77 and 300 K. At 300 K, the spectra show evidence for a close to axial site symmetry.

A first-order phase transition occurs at about 350 K, with the advent of new lines and the merging of others. At 370 K, the degeneracy of ^7F_J and ^5D_J levels is still partially lifted. Table 5 gives the number of observed lines in the explored spectral range compared to the number of allowed transitions in a D_{2d} site symmetry. It can be stated that for nine out of thirteen transitions the number of observed lines matches exactly the number of allowed ones. In the four remaining cases, $^5D_0 \rightarrow {}^7F_5$, $^5D_0 \rightarrow {}^7F_6$, $^5D_1 \rightarrow {}^7F_3$ and $^5D_1 \rightarrow {}^7F_4$ which are rather weak transitions, 3, 4, 6 and 5 lines are observed instead of 4, 5, 8, and 10 allowed. Therefore, on the whole, the observed selection rules are in agreement with a D_{2d} site symmetry. The $^5D_0 \rightarrow {}^7F_0$ transition is forbidden (and not observed) and the $^5D_0$ energy level is deduced from the observations of $^5D_0 \rightarrow {}^7F_1$, $^5D_1 \rightarrow {}^7F_0$, and $^5D_1 \rightarrow {}^7F_1$.

In Ref. (20), it was stated that a tetragonal form of $LiYO_2$:Eu^{3+} was obtained as a metastable phase after heating at 1200°C and that it was less efficient than the monoclinic form. We never obtained a metastable tetragonal form at room temperature. Figure 4 shows the spectra at 300 and at 370 K, just beyond the phase transition. There is no distinct change in the intensity of the $^5D_0\,(A_1) \rightarrow {}^7F_2\,(B_2)$ transition at about 16,316 cm^{-1} (613 nm) except a decrease of the maximum peak height compensated by the line broadening. A compression of the $^5D_0\,(A_1) \rightarrow {}^7F_2\,(E)$ component is visible leading to a slight decrease of the total $^5D_0 \rightarrow {}^7F_2$ intensity.

It seems that the energy levels which do not shift smoothly throughout the transition are those with symmetry levels B_1 for J even and A_2 for J odd. It is difficult to check this for $J = 5$ and 6. The energy levels at these three temperatures are indicated in Table 6 (see also Fig. 5). The $^5D_3$ levels have been deduced from sharp $^5D_3 \rightarrow {}^7F_J$ ($J = 0, 1, 2$) lines observed at 77 K in the second order of the analyzing monochromator. These lines appear in the 11,600–12,200 cm^{-1} region, which is in the first-order $^5D_0 \rightarrow {}^7F_6$ region. The excitation of the $^5D_3$ levels can be ascribed to one of the following up-converting mechanisms:

—A two-photon absorption from $^7F_0$ up to the $4f^7 2p5$ charge-transfer band followed by a decay down to $^5D_3$ and an emission back to $^7F_0$.

—First, the excitation of a $4f$ electron to $^5D_2$ followed by the emission of $^5D_2 \rightarrow {}^7F_4$; second, the reabsorption from the excited $^7F_4$ state up to $^5D_3$ and a final emission toward the ^7F_J.

The latter mechanism seems the most probable since it can be checked from Table 6 that two combinations of $^7F_4$ and $^5D_2$ sublevels match exactly the energies of $^5D_3$ sublevels, i.e.,

$^5D_3$		$^5D_2$		$^7F_4$	(cm^{-1})
24202	=	21452	+	2750	
24162	=	21303	+	2956.	

At room temperature, the lifetimes of the $^5D_0$, $^5D_1$, and $^5D_2$ are equal to 930, 50, and about 7 μs, respectively.

IV.2. $LiYO_2$:Tb^{3+}

When illuminated with the short 254-nm wavelength of the mercury lamp the compound $LiYO_2$:Tb^{3+} produces a strong green luminescence originating mainly from the $^5D_4 \rightarrow {}^7F_5$ transition.

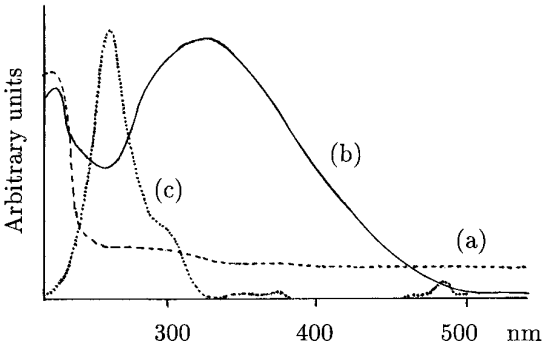

FIG. 6. Absorption spectrum of (a) pure $LiYO_2$ and (b) $LiYO_2$:Tb^{3+}; (c) excitation spectrum of $LiYO_2$:Tb^{3+} (observation at 543 nm).

A global excitation spectrum was recorded by means of a Kontron spectrofluorimeter measuring the output of the strong $^5D_4 \rightarrow {}^7F_5$ transition and exciting with a xenon lamp from 200 to 550 nm. It is represented in Fig. 6 with the absorption spectrum of the compound and of pure $LiYO_2$ recorded with a Varian spectrophotometer Cary 5E. The most efficient excitation occurs for the wavelength where the matrix absorption overlaps the $4f \rightarrow 5d$ absorption band (263 nm).

The optical spectra of $LiYO_2$:Tb^{3+} were recorded utilizing the same selective excitation technique as described above. The experiments were done at 20 K by using a He closed cycle cryostat (model CP-62-ST/5 from Cryophysics).

Eight out of the nine Stark components of $^5D_4$ were determined by means of an excitation spectrum monitored by the strongest $^5D_4 \rightarrow {}^7F_5$ emission. A selective excitation of the lowest $^5D_4$ component at 20,556 cm^{-1} yields the fluorescence lines emitted by this particular level (1), but also from higher ones situated at 20 (2), 35 (3), and 54 (4) cm^{-1} above. The lifetime of the lowest is equal to 1470 μs at 20 K. The lifetime of the two upper components is about

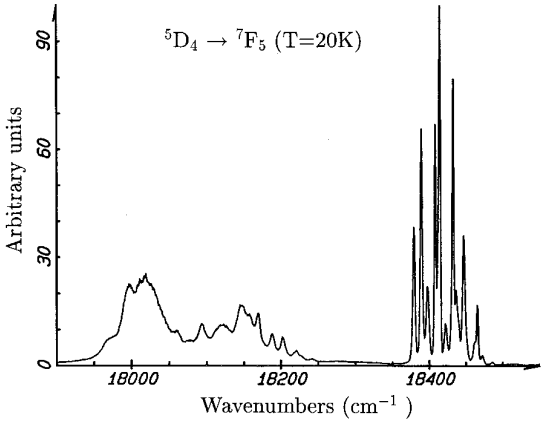

FIG. 7. $^5D_4 \rightarrow {}^7F_5$ emission of $LiYO_2$:Tb^{3+} (excitation at 20,556 cm^{-1}).

TABLE 7
Experimental and Calculated Energy Levels (in cm^{-1}) of $LiYO_2$:Tb^{3+} at 20 K

	Exp.	Cal.
$^7F_6$	0	0
	26	18
	41	60
	/	97
	108	113
	164	157
	173	172
	/	464
	/	503
	/	570
	588	585
	646	643
	/	665
$^7F_5$	2144	2140
	2168	2161
	2178	2188
	2387	2378
	2409	2412
	2435	2437
	/	2477
	2517	2528
	/	2530
	2583	2580
	2590	2584
$^7F_4$	3377	3376
	3437	3428
	3471	3475
	3484	3490
	3566	3559
	3615	3617
	3855	3855
	3932	3927
	3949	3958
$^7F_3$	/	4523
	4564	4565
	4585	4572
	4606	4603
	4627	4626
	/	4665
	4792	4799
$^7F_2$	5282	5279
	5331	5338
	5385	5397
	5568	5558
	5601	5597
$^7F_1$	5747	5763
	5846	5835
	5903	5897
$^7F_0$	6138	6138

TABLE 7—*Continued*

	Exp.	Cal.
$^5D_4$	20556	
	20576	
	20591	
	20610	
	20617	
	20632	
	20697	
	20719	

1/2 that of the lowest one; a fact which cannot be explained by the plain hypothesis of thermal equilibrium, yet it enabled us to determine unambiguously the Stark components of the ^7F_J ($J = 0, 1, 2, 3, 4, 5, 6$) levels. Figure 7 represents the $^5D_4 \rightarrow {}^7F_5$ transition at 20 K. The ^7F_J ($J = 0 \rightarrow 6$) and $^5D_4$ energy levels are listed in Table 7.

V. CRYSTAL FIELD ANALYSIS

The matrix elements of the one-particle crystal field and an approximate spin–orbit interaction acting between the ^7F_J ($J = 1, 6$) levels is given by

$$\langle J, M \,|\, H \,|\, J', M' \rangle = \left\langle J, M \left| \sum_{k,q} B_q^k \sum_i C_q^k(i) \right| J', M' \right\rangle + A(J) \cdot \delta(J, J') \cdot \delta(M, M'). \quad [2]$$

The adjustable $A(J)$ values fix the levels barycenters.

The yttrium randomly substituted by europium or terbium occupies a C_1 site, consisting in a distorted cubic (oxygen octahedron) site.

A C_1 crystal field analysis involves the eventual fit of at most 27 crystal field parameters (*cfp*). As mentioned above, signals of the characteristic cubic degeneracies can be seen in the experimental fluorescence spectra of the europium doped compound at 300 K. Therefore, the symmetry is not too far from cubic and there exist possibilities for some of the *cfp* to be small. In order to select the relevant *cfp*, *ab initio* values were calculated by the covaloelectrostatic model along the lines developed in Ref. (33). It consists of adding an electrostatic and a covalent component.

The electrostatic components of the *cfp* with $k = 2$ and 4 are calculated by the means of program CHLOE (34) with an oxygen charge equal to -0.7 (35).

The covalent contribution is evaluated after selecting the ionization energy of the two oxygen species according to the rare earth–ligand distance (Ref. (34), Fig. 1). In a cubic site symmetry, there are three equivalent mutually perpendicular fourfold axes. Three pseudo-fourfold axes exist also at the yttrium site of the $LiYO_2$ structure. The semi-empirical *cfp* were calculated in the three coordinate systems and we selected the one displaying the smallest q odd parameters. It was obtained by rotating the structure by 30°, 90°, and 143° around Oz, Oy, and Oz (old axes) successively. The electrostatic contribution is calculated for first neighbors only.

The electrostatic and covalent contributions, as well as

TABLE 8
Electrostatic and Covalent Contributions to the *cfp* Calculated by the Covaloelectrostatic Model (italic), Total Predicted Crystal Field Parameters in the Monoclinic and Tetragonal Phases Compared with Experimentally Fitted *cfp*

	$P2_1/c$ (C_1)					$I4_1/amd$ (D_{2d})	
	Tb^{3+}	Eu^{3+}				Eu^{3+}	
	20 K	77 K	300 K			370 K	
	Exp	Exp	$C - E$		Exp	$C - E$	Exp
cm^{-1}							
B_0^2	−185(10)	−236(9)	*−403*	(*−280−123*)	−370(12)	*−1036* (*−809−227*)	−603(10)
B_1^2	229(7)	160(16)	*210*	(*130+80*)	133(29)		
S_1^2		−215(7)	*105*	(*55+50*)	−197(9)		
B_2^2	83(8)	−93(21)	*350*	(*243+107*)	−57(23)		
B_0^4	2302(23)	2323(60)	*1989*	(*521+1468*)	2377(96)	*2380* (*564+1816*)	2852(20)
B_1^4	−498(42)	116(19)	*345*	(*85+260*)	38(24)		
S_1^4	−360(15)	−372(20)			−215(24)		
B_4^4	1613(24)	1520(17)	*1440*	(*355+1085*)	1536(21)	*1760* (*382+1378*)	2019(20)
B_0^6	413(15)	633(16)	*423*		559(27)	*412*	234(35)
B_4^6	−363(49)	−629(36)	*−527*		−677(52)	*−761*	−914(28)
S_4^6		464(27)			478(35)		
rms	9.6	9.4			11.9		14.8
Levels	40	43			38		36

the total predicted parameters for the monoclinic phases calculated with the structural data at 300 K in the defined reference frame are given in Table 8. We have only taken into account the parameters larger than 60 cm^{-1}, i.e., B_0^2, B_1^2, S_1^2, B_2^2, B_0^4, B_4^4, B_0^6, B_4^6, and S_4^6. Given also are the predicted parameters of the tetragonal phase utilizing the structural data at 370 K (Table 3).

The experimental *cfp* values were refined by means of program SEPTF allowing the adjustment of the ^7F_J manifold, starting from the parameters determined in the former step. They are reported in Table 8 for both structural forms. At 77 and 300 K, but mainly at 300 K, the overwhelmingly strong *cfp* are those allowed in the high temperature phase.

VI. CONCLUSION

We have undertaken a crystallographic and optical study on europium and terbium doped lithium yttriate in powder form. At room temperature, the crystal symmetry is monoclinic or tetragonal whether the doping rare earth is trivalent (Eu^{3+} or Tb^{3+}) or tetravalent (Tb^{4+}). The monoclinic form of $LiYO_2$:Eu^{3+} transforms into the tetragonal form at about 350 K. At the transformation, the major change is a 2.3% contraction of the *c* axis of the pseudo-tetragonal cell. The crystal structures of the samples were examined and the condition determining whether the compound is monoclinic or tetragonal at room temperature is given. The investigated compounds are good phosphors and their cathodoluminescent efficiency was investigated. The radiances of the europium and terbium compound are 0.33 and 0.47 times that of the commercial television standards Y_2O_2S:Eu^{3+} and ZnS:Cu,Al, respectively. The two phosphors are stable at room temperature but are decomposed by heating at 400°C under the normal conditions for manufacturing cathode-ray screens. We are currently undertaking a systematic study of the decomposition process.

Crystal field parameters were predicted and compared with empirical fitted values. Considering the strength of the crystal field, the ratio $E_4/|E_2 + E_6|$ is equal to 2.21 and 2.57 in the monoclinic and tetragonal phases, respectively, which are to our knowledge the highest known values. This ratio, usually high for efficient phosphors, is equal to 1.26, 1.40, and 1.89 for Eu^{3+} doped in YVO_4, Y_2O_3, and Y_2O_2S, respectively.

REFERENCES

1. R. Hoppe, *Angew. Chem.* **71,** 457 (1959).
2. R. Hoppe and H. J. Rohrborn, private communication.
3. F. Bertaut and M. Gondrand, *C.R. Acad. Sci.* **255,** 1135 (1962).
4. H. Glaum, S. Voigt, and R. Hoppe, *Z. Anorg. Allg. Chem.* **598/599,** 129 (1991).
5. F. Stewner and R. Hoppe, *Z. Anorg. Allg. Chem.,* **380,** 250 (1971).
6. N. I. Sevost'yanova, I. A. Murav'eva, L. M. Kovba, L. I. Martynenko, and V. I. Spitsyn, *Dokl. Akad. Nauk SSSR* **161,** 1359 (1965).
7. H. Bärnighausen, *Acta Crystallogr.* **16,** 1073 (1963).
8. M. Gondrand and F. Bertaut, *Bull. Soc. Fr. Minéral Cristallogr.* **86,** 301 (1963).
9. M. Gondrand, *Bull. Soc. Fr. Minéral. Cristallogr.* **96,** 166 (1973).
10. H. Bärnighausen, *Acta Crystallogr.* **19,** 1048 (1965).
11. M. Gondrand, *Bull. Soc. Fr. Minéral. Cristallogr.* **90,** 107 (1967).
12. M. Gondrand, *Bull. Soc. Fr. Minéral. Cristallogr.* **93,** 421 (1970).
13. M. Waintal and M. Gondrand, *Mater. Res. Bull.* **2,** 889 (1967).
14. B. E. Zaitsev, B. N. Ivanov-Emin, V. M. Akimov, E. N. Siforova, and V. Miliado Campos, *Zh. Strukt. Khim.* **11,** 686 (1970).
15. I. A. Rozdin, H. T. Saripov, S. S. Plotkin, N. V. Brotnikov, T. B. Polueva, and K. I. Petrov, *Izv. Akad. Nauk SSSR Neorg. Mater.* **12,** 863 (1976).
16. G. Blasse, *J. Chem. Phys.* **45,** 2356 (1966).
17. G. Blasse and A. Bril, *J. Chem. Phys.* **45,** 3327 (1966).
18. G. Blasse, A. Roos, and A. C. Van der Steen, *J. Solid State Chem.* **24,** 233 (1978).
19. L. H. Brixner, *J. Electrochem. Soc. Solid State Sci.* **114,** 252 (1967).
20. P. M. Jaffe and J. D. Konitzer, *J. Electrochem. Soc.* **116,** 633 (1969).
21. M. Blanchard, C. Linarès, and F. Gaume-Mahn, *C.R. Acad. Sci. Paris Ser. B* **271,** 523 (1970).
22. F. Gaume-Mahn, C. Linarès, and M. Blanchard, *Proc. 9th Rare Earth Res. Conf.* **2,** 478 (1971).
23. V. A. Antonov and P. A. Arsenev, *Phys. Status Solidi A* **32,** K71 (1975).
24. V. A. Antonov, P. A. Arsenev, S. A. Vakhidov, E. M. Ibragimova, and D. S. Petrova, *Phys. Status Solidi A* **41,** 45 (1977).
25. V. A. Antonov, P. A. Arsenev, Z. A. Artykov, and D. S. Petrova, *Zh. Prikl. Spektrosk.* **31,** 1106 (1979).
26. M. Faucher, O. K. Moune, L. Albert, and B. Piriou, *C. R. Acad. Sci. Paris II* **317,** 1569 (1993).
27. E. S. Kuli-Zade and N.S. Shuster, *Azerb. Khim. Zh.* **5,** 115 (1983).
28. N. S. Shuster and E. S. Kuli-zade, *Inorg. Mater.* **24,** 435 (1988).
29. S. P. Sinha, "Complexes of the Rare Earths," Pergamon, Oxford, 1966.
30. R. D. Shannon, *Acta Crystallogr. Sect. A* 751 (1976).
31. J. F. Bérar and P. Garnier, "APD 2nd Conference." Natl. Inst. Science and Technology, Gaithersburg, May 1992.
32. B. Piriou, J. Dexpert-Ghys, and S. Mochizuki, *J. Phys. Condens. Matter* **6,** 7317 (1994).
33. D. Garcia and M. Faucher, *J. Chem. Phys.* **82,** 5554 (1985).
34. M. Faucher, Program CHLOE in "Logiciels pour la Chimie" Vol. 60. ANL-SFC, 1991.
35. M. Faucher, D. Garcia, and O. K. Moune, *J. Lumin.* **51,** 341 (1992).